

The importance of EBIT data for Z-pinch plasma diagnostics¹

A.S. Safronova, V.L. Kantsyrev, P. Neill, U.I. Safronova, D.A. Fedin, N.D. Ouart, M.F. Yilmaz, G. Osborne, I. Shrestha, K. Williamson, T. Hoppe, C. Harris, P. Beiersdorfer, and S. Hansen

Abstract: The results from the last six years of X-ray spectroscopy and spectropolarimetry of high-energy density Z-pinch plasmas complemented by experiments with the electron beam ion trap (EBIT) at the Lawrence Livermore National Laboratory (LLNL) are presented. The two topics discussed are the development of M-shell X-ray W spectroscopic diagnostics and K-shell Ti spectropolarimetry of Z-pinch plasmas. The main focus is on radiation from a specific load configuration called an “X-pinch”. In this work the study of X-pinch with tungsten wires combined with wires from other, lower Z materials is reported. Utilizing data produced with the LLNL EBIT at different energies of the electron beam the theoretical prediction of line positions and intensity of M-shell W spectra were tested and calibrated. Polarization-sensitive X-pinch experiments at the University of Nevada, Reno (UNR) provide experimental evidence for the existence of strong electron beams in Ti and Mo X-pinch plasmas and motivate the development of X-ray spectropolarimetry of Z-pinch plasmas. This diagnostic is based on the measurement of spectra recorded simultaneously by two spectrometers with different sensitivity to the linear polarization of the observed lines and compared with theoretical models of polarization-dependent spectra. Polarization-dependent K-shell spectra from Ti X-pinch plasmas are presented and compared with model calculations and with spectra generated by a quasi-Maxwellian electron beam at the LLNL EBIT-II electron beam ion trap.

PACS Nos.: 32.30.Rj, 52.58.Lq, 52.70.La

Résumé : Nous présentons les résultats des six dernières années en spectroscopie des rayons-X et en spectropolarimétrie des plasmas à striction Z de haute densité d'énergie, complétés par les expériences faites avec le piège ionique à faisceau d'électrons (EBIT) du Lawrence Livermore National Laboratory (LLNL). Les deux sujets analysés sont le développement de diagnostics spectroscopiques de rayons-X dans la couche M du W et la spectropolarimétrie de plasmas à striction Z du Ti. Nous nous concentrons sur la radiation provenant d'une configuration particulière appelée striction X. Nous étudions ici des strictions X avec des fils de W combinés avec des fils de matériaux de Z plus bas. Utilisant les données produites au EBIT à différentes énergies du faisceau d'électrons, nous testons et calibrons la position et l'intensité des lignes de la couche M du W. Les expériences de striction X sensibles à la polarisation faites à l'Université du Nevada à Reno (UNR) fournissent la preuve expérimentale de l'existence de forts faisceaux d'électrons dans les plasmas à striction X de Ti et de Mo et justifient le développement de la spectropolarimétrie des rayons-X dans les plasmas à striction Z. Ce diagnostic est basé sur les mesures de spectres enregistrés simultanément par deux spectromètres avec des sensibilités différentes à la polarisation linéaire des lignes observées et comparées avec des modèles théoriques de spectres dépendant de la polarisation. Nous présentons des spectres dépendant de la polarisation dans la couche K du Ti en striction X et les comparons avec des calculs de modèles théoriques et avec des spectres générés par un faisceau d'électrons quasi maxwellien au piège ionique à faisceau d'électrons EBIT-II du LLNL.

[Traduit par la Rédaction]

1. Introduction

The electron beam ion trap (EBIT) is an excellent source for bench-marking of the non-local thermodynamic equilibrium (non-LTE) kinetic modeling as well as new spectroscopic diagnostics of plasmas because it is capable of producing X-ray lines

using a beam of non-Maxwellian electrons at well-controlled experimental conditions, which include, for example, selection of the atomic process, ionization stage, and the energy of the electron beam. Two different topics are covered in this paper which is the analysis of M-shell W radiation and K-shell Ti ra-

Received 6 March 2007. Accepted 5 June 2007. Published on the NRC Research Press Web site at <http://cjp.nrc.ca/> on 9 February 2008.

A.S. Safronova,² V.L. Kantsyrev, P. Neill, U.I. Safronova, D.A. Fedin, N.D. Ouart, M.F. Yilmaz, G. Osborne, I. Shrestha, and K. Williamson. Physics Department, MS 220, University of Nevada, Reno, NV 89557, USA.

T. Hoppe. Physics Department, MS 220, University of Nevada, Reno, NV 89557, USA; Drexel University, PA 19104, USA.

C. Harris. Gulf Coast Community College, Panama City, FL 32401, USA.

P. Beiersdorfer and S. Hansen. Lawrence Livermore National Laboratory, Livermore, CA 94550, USA.

¹Paper given at the Workshop on Twenty Years of Spectroscopy with EBIT held in Berkeley, California, 13–15 November 2006.

²Corresponding author (e-mail: alla@physics.unr.edu).

diation from LLNL EBIT and UNR X-pinch experiments. The advantages provided by the electron beam ion trap data in the interpretation of X-pinch spectra are presented.

The first X-ray spectra of M-shell W were produced by high-density exploded-wire plasmas more than 25 years ago [1]. The precision of the measurements of Ni-like W lines was improved in laser plasma experiments [2]. The extended analysis of Ni-like W spectra from laser plasma has included $nf \rightarrow 3d$ ($n = 5-9$), $nd \rightarrow 3p$ ($n = 4-6$), and $np \rightarrow 3s$ ($n = 4, 5$) transitions [3]. Tungsten wire arrays have been studied extensively on the Z accelerator at Sandia National Laboratories (SNL) since 1998 when it was shown that they can produce X-ray powers up to 200 TW and X-ray energies up to 2 MJ [4, 5]. Since then, despite an increasing number of papers about the implosions of W arrays on the SNL-Z machine and their recent applications to inertial confinement fusion [6, 7], X-ray M-shell diagnostics of tungsten high-energy density (HED) plasmas have not yet been developed.

In this paper, we present a theoretical model of M-shell W spectra. This model was bench-marked with LLNL EBIT data produced at different energies of the electron beam and recorded by crystal spectrometers and a broadband microcalorimeter. Moreover, high-temperature and high-density plasmas were produced from the variety X-pinch on a 1 MA Zebra device at UNR. In particular, M-shell W radiation was generated by the implosions of X-pinch with tungsten wires combined with the wires from other lower Z wire material such as Al and Mo. These data are also presented.

X-pinch is an excellent source for testing new spectral diagnostics and for atomic modelling because of the high density ($> 10^{21} \text{ cm}^{-3}$) and temperatures ($> 1 \text{ keV}$) of the pinch plasmas, which scale from a few μm to several mm in size. They offer a variety of load configurations, which differ in wire connections, number of wires, and wire materials. An X-pinch plasma is formed by touch-crossing two wires between the electrodes of a high-current pulsed-power generator. The current quickly vaporizes and strongly ionizes the wire material. As a result, an X-pinch yields short X-ray bursts from one or more small bright spots at the intersection of the crossed wires.

Currently, X-ray spectra of X-pinch are collected and studied at different pulsed-power machines, for example, at the university-scale 1 MA Zebra device at University of Nevada, Reno [8–12] and Cobra facility at Cornell University (CU) [11, 12], as well as at smaller devices such as at a 450 kA pulsed-power device at CU [13]. It was shown that X-pinch plasmas can reach temperatures of 2–3 keV and densities up to 10^{23} cm^{-3} . Another distinct feature of X-pinch is the existence of plasma anisotropy in the form of strong electron beams, which makes them attractive objects for spectropolarimetry (a powerful tool for studying the anisotropy of high-temperature plasmas). The structure of 1 MA driven X-pinch is complicated and includes energetic electron beams directed toward the center of the X-pinch anode between the wires and along the wires towards the anode. Several experimental observations such as holes in the anode, X-rays with energies more than 3.5 keV directed towards the anode from pinhole images, and “cold” characteristic lines with energies at least 3–5 keV (for Ti) evidence the presence of such electron beams (see, for example, refs. 14 and 15).

Because of the high temperature and density, polarized emission from an X-pinch plasma is complicated. We started with investigation of the polarization properties of K-shell Ti lines

using the LLNL EBIT. Our previous work on X-ray line polarization at LLNL EBIT included the study of polarization-dependent spectra of X-ray dielectronic satellites of Li- and Be-like [16, 17] and B-like Fe ions [18]. In the present paper, we analyze polarization-dependent Ti K-shell spectra generated by a quasi-Maxwellian electron beam at the LLNL EBIT and compare this analysis with K-shell spectra from Ti X-pinch obtained at UNR.

2. M-shell W radiation from LLNL EBIT and UNR X-pinch experiments

2.1. M-shell W model: atomic and plasma physics in the model

Our new non-LTE collisional radiative (CR) model of the M-shell W emission has about 4000 levels, and includes the ground states from all ions from neutral to bare W and a detailed structure for Cr-like to Se-like W ions. It is similar to the model recently developed and used in ref. 11, but has more high Rydberg levels of Ni-like W. Each fine-structure state is linked to other states within its ionization state through collisional excitation, de-excitation, and radiative decay. All the states of the ions are linked via collisional ionization, three-body recombination, and radiative recombination. The energy-level structure and complete radiative coupling as well as a subset of collisional data for Cr-like to Se-like W ions were calculated using the Flexible Atomic Code (FAC) developed by Gu [19]. To limit the enormous amount of input data but to keep the complete collisional coupling among excited levels, the modified Van Regemorter approximation [20] was used to calculate the excitation cross sections (which can lead to some overestimation in the electron temperature) as well as a modified Lotz formula [21] to calculate the ionization cross sections.

The energies for the excited states for the transitions $3l-4l'$, $3l-5l''$, and $3l-6l'''$ as well as radiative transition probabilities in Ni-like W were also determined to second order in Relativistic Many Body Perturbation Theory (RMBPT) [22–24]. The calculations start from a closed-shell Dirac–Fock potential, and include second-order Coulomb and Breit–Coulomb interactions. Electric-dipole matrix elements are calculated in second order for transitions from excited states to the ground state. Table 1 lists the atomic data calculated for the most intense lines in Ni-like W specified in LS coupling. In particular, the spectral lines Ni1–Ni10 are allowed electric-dipole (E1) transitions, i.e., transitions of the type 3–6 (Ni1, Ni2), 3–5 (Ni3 and Ni4), and 3–4 (Ni5–Ni10). The spectral lines Ni11 and Ni12 are forbidden 3–4 electric-quadrupole (E2) transitions. The comparison of RMBPT and FAC atomic data calculated for the observable transitions in Ni-like W in Table 1 shows a good agreement. Only FAC data were used for the modeling discussed in the next sections.

2.2. Modeling of the M-shell W spectra from the LLNL EBIT

M-shell W spectra produced at the LLNL EBIT-I and EBIT-II electron beam ion traps were collected in two different experiments using a crystal spectrometer and an X-ray spectrometer (XRS) microcalorimeter from the Suzaku X-ray satellite mission. In the experiments that employed a crystal spectrometer on EBIT-II, the M-shell W spectra were produced at 11 different values of the electron beam energy (E_b) ranging from 2.4 to

Table 1. Wavelengths (λ in \AA) and radiative transition rates (Ar in s^{-1}) for the strongest E1 and E2 transitions from excited states with $J = 1$ and 2 into the ground state in Ni-like W calculated by Relativistic Many Body Perturbation Theory (RMBPT) [22–24] and Flexible Atomic Code (FAC) [19] codes.

Line	Upper level	RMBPT		FAC	
		$\lambda(\text{\AA})$	Ar (s^{-1})	$\lambda(\text{\AA})$	Ar (s^{-1})
Ni1	$3d6f^1P_1$	3.803	5.30[13]	3.805	6.51[13]
Ni2	$3d6f^3D_1$	3.879	5.66[13]	3.880	7.25[13]
Ni3	$3d5f^1P_1$	4.308	1.16[14]	4.309	1.33[14]
Ni4	$3d5f^3D_1$	4.403	9.07[13]	4.405	1.02[14]
Ni5	$3p4d^1P_1$	5.201	9.35[13]	5.195	9.54[13]
Ni6	$3p4s^1P_1$	5.689	3.72[14]	5.686	3.99[14]
Ni7	$3d4f^3D_1$	5.870	1.18[14]	5.872	1.24[14]
Ni8	$3d4f^3P_1$	6.154	2.21[13]	6.144	2.17[13]
Ni9	$3d4p^3D_1$	7.027	1.27[13]	7.028	1.21[13]
Ni10	$3d4p^3P_1$	7.174	6.67[12]	7.175	6.32[12]
Ni11	$3d4s^1D_2$	7.608	4.04[09]	7.610	4.55[09]
Ni12	$3d4s^3D_2$	7.929	5.32[09]	7.930	5.97[09]

4.6 keV. This spectrometer covered the spectral region from 5 to 6 \AA with a spectral resolution of 2200. The analysis of these spectra was given in ref. 25. Here, we show some of these spectra and make a comparison with our new non-LTE model. In particular, the experimental M-shell W spectra recorded with the crystal spectrometer and produced at $E_b = 3.6, 3.9,$ and 4.3 keV are presented along with our modeling results in Figs. 1–3, respectively. The Ni-like W lines Ni6, Ni7, and Ni5 dominate the spectra produced at $E_b = 3.6$ and 3.9 keV (see Figs. 1 and 2), and the Cu-like lines Cu1 and Cu2 are much less intense than the Ni-like lines. Moreover, the two M-shell W spectra are almost the same for these two electron beam energies. By contrast, the spectrum at $E_b = 4.3$ keV is different (see Fig. 3). Though the same three Ni-like lines are still intense, spectral lines from higher ionization stages (Co1, Co2, and Fe1) appear because this electron beam energy exceeds the ionization potential of Ni- and Co-like W. The non-LTE W model calculates not only spectra within one ionization state but also charge-state distribution. In general, modeling (top) reproduces the experimental spectra well (bottom) in all three figures as discussed early in ref. 26. In particular, the comparison is very good for Ni-like (Figs. 1–3) and for nearby ionization states such as Cu-like (Fig. 2) and Co- and Zn-like (Fig. 3) W ions.

The XRS microcalorimeter as fielded on EBIT-I was capable of acquiring, filtering, and characterizing X-ray events on 32 independent pixels as described in refs. 27 and 28. This spectrometer calorimeter recorded the spectra in a broader spectral range (from 3 to 8 \AA) and with about six times less resolution than the crystal spectrometer. In these experiments only 14 pixels were used, and each pixel functioned simply as one of 14 independent spectrometers. The good reproducibility of the spectra from pixel to pixel was observed. In Fig. 4, the experimental spectrum (bottom) from one of the pixels recorded by the XRS microcalorimeter at $E_b = 3.9$ keV is presented along with the modeling (top). This spectrum is similar to the one recorded by the crystal spectrometer in Fig. 2 but covers a broader spectral range from 3 to 9 \AA . As a result, it includes not only the three lines Ni6, Ni7, and Ni5 but also the other Ni-like

Fig. 1. Experimental M-shell spectrum of W ions from the LLNL EBIT-II facility recorded by a crystal spectrometer at $E_b = 3.6$ keV (bottom) and theoretical synthetic spectrum calculated for a Gaussian electron distribution function of FWHM = 50 eV centered at 3.6 keV (top). Intense spectral features are identified by the iso-electronic sequence.

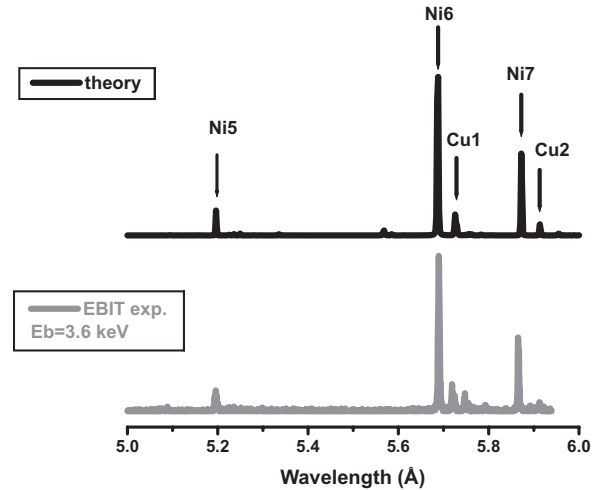
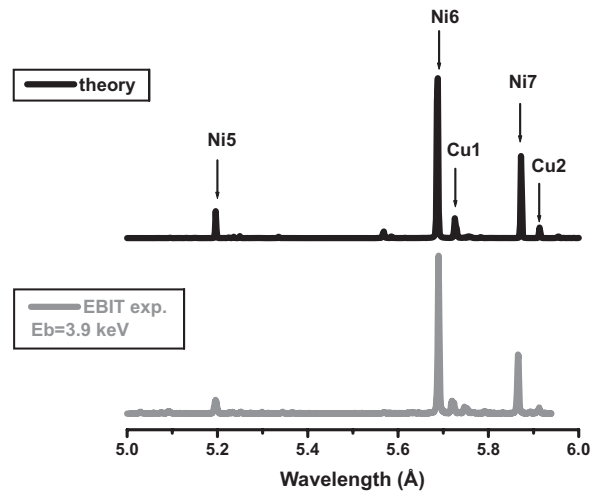


Fig. 2. Experimental M-shell spectrum of W ions from the LLNL EBIT-II facility recorded by a crystal spectrometer at $E_b = 3.9$ keV (bottom) and theoretical synthetic spectrum calculated for a Gaussian electron distribution function of FWHM = 50 eV centered at 3.9 keV (top). Intense spectral features are identified by the iso-electronic sequence.



lines from Table 1. The theoretical synthetic spectrum at the top of Fig. 4 is calculated using the non-LTE kinetic model of W with a Gaussian electron distribution function of 50 eV FWHM centered at $E_b = 3.9$ keV. This is the same as the one used for the synthetic spectrum in Fig. 2. All 12 lines Ni1–Ni12 are reproduced well by our theory.

2.3. Comparison of the M-shell W spectra from the LLNL EBIT and UNR X-pinch experiments and modeling of the UNR X-pinch experiments

X-pinch experiments with tungsten wires combined with wires from other, lower Z wire material such as Al and Mo were used in experiments on the 1MA pulsed-power generator Zebra at UNR to produce and study M-shell radiation from W ions. We have

Fig. 3. Experimental M-shell spectrum of W ions from the LLNL EBIT-II facility recorded by a crystal spectrometer at $E_b = 4.3$ keV (bottom) and theoretical synthetic spectrum calculated for a Gaussian electron distribution function of FWHM = 50 eV centered at 4.3 keV (top). Intense spectral features are identified by the iso-electronic sequence.

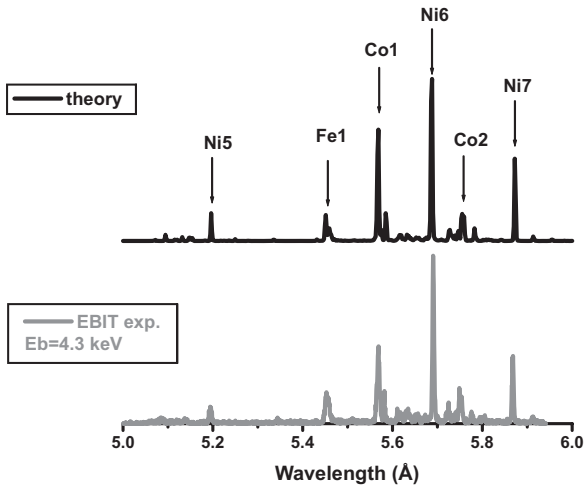
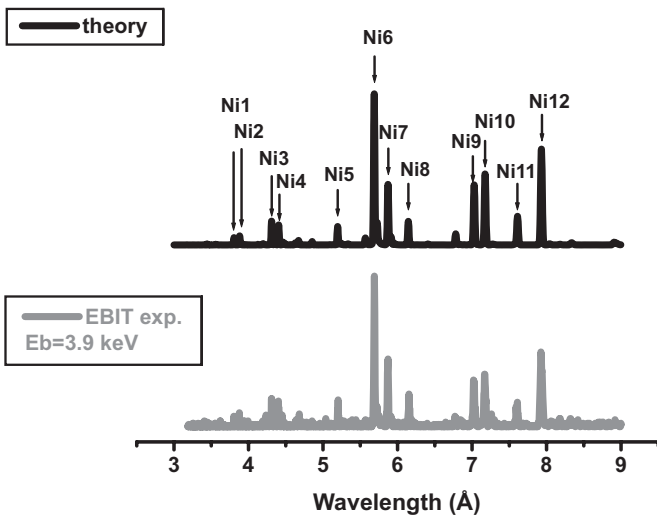
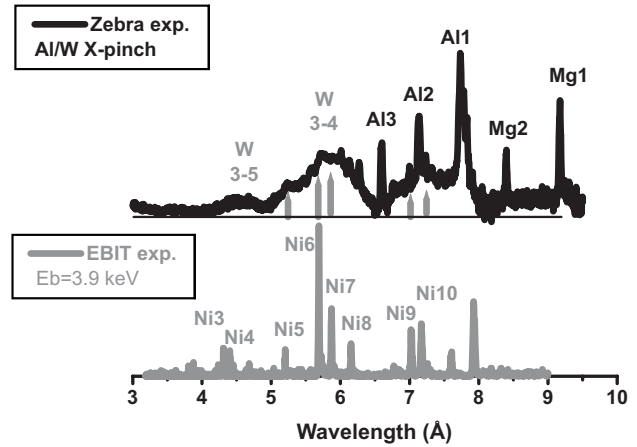


Fig. 4. Experimental M-shell spectrum of W ions from the LLNL EBIT-I device recorded by the X-ray spectrometer microcalorimeter at $E_b = 3.9$ keV (bottom) and theoretical synthetic spectrum calculated for a Gaussian electron distribution function of FWHM = 50 eV centered at 3.9 keV (top). Intense spectral features are identified by the iso-electronic sequence.



found that using combined X-pinch configurations consisting of one or a few W wires and the rest of the wires from a lower Z material (such as Mo or Al) provides better quality M-shell W spectra than when using only W wires [11, 12]. The experimental Al/W X-pinch spectrum is shown at the top of Fig. 5. It was a planar-loop X-pinch with a 99 μm Al 5056 wire in the anode loop and a 35 μm W wire in the cathode loop. The experimental spectrum includes both K-shell radiation from Al and Mg (Al 5056 has 95% Al and 5% Mg) and M-shell radiation from W. The line designation for all K-shell lines (Al, Mg, and Ti) is the same throughout the paper. For example, Al1 is the He_α line, Al2 is

Fig. 5. Experimental spectrum from the Zebra Al/W X-pinch (top) and experimental M-shell spectrum of W ions from the LLNL EBIT-I electron ion beam trap recorded by the X-ray spectrometer microcalorimeter at $E_b = 3.9$ keV (bottom).



the Ly_α line, and Al3 is the He_β line of Al for K-shell Al.

EBIT spectra were very useful in the identification of M-shell W spectra from the implosion of combined X-pinch configurations. The comparison of the Al/W X-pinch spectrum (Fig. 5, top) with the experimental LLNL EBIT spectrum (bottom of Figs. 4 and 5) reveals the 3–4 transitions (Ni5–Ni10) and 3–5 transitions (Ni3 and Ni4) in Ni-like W.

The experimental W/Mo X-pinch spectrum is shown at the top of Fig. 6. It was a planar-loop X-pinch with a 35 μm W wire in the anode loop and a 50 μm Mo wire in the cathode loop. The experimental spectrum includes both L-shell radiation from Mo and M-shell radiation from W. The comparison of the W/Mo X-pinch spectrum (Fig. 6, top) with the experimental LLNL EBIT spectrum (bottom of Figs. 4–6) reveals the 3–4 transitions (Ni5–Ni10). Because 3–5 transitions in Ni-like W overlap with 2–3 transitions in L-shell Mo, the lines Ni3 and Ni4 could not be assigned to particular peaks in this X-pinch spectrum. Figure 7 shows the M-shell W modeling of the above mentioned combined X-pinch spectra at an electron temperature $T_e = 1$ keV, electron density $N_e = 10^{21} \text{ cm}^{-3}$, and a small portion of non-Maxwellian electrons $f = 0.03$ (for more about the influence of hot electrons on X-ray spectra, see, for example, refs. 29 and 30). Modeling describes the most intense peaks and the ratio between 3–5 and 3–4 transitions in Ni-like W well. However, more work is needed to match the intensities of higher and lower ionization stages. It is important to note that forbidden E2 transitions Ni11 and Ni12, which are present in spectra from low-density sources, are not observed in the X-pinch spectra.

3. K-shell Ti radiation from the LLNL EBIT and UNR X-pinch experiments

K-shell Ti lines important for diagnosing low-density plasmas are listed in Table 2. They include the He-like lines, in particular the He_α resonance line (w), the intercombination line IC (y), the forbidden lines x and z, and the inner-shell satellite lines of Li-like ions q and r. All these lines are often used in the diagnostics of Ti plasmas from tokamaks [31, 32] and electron beam ion traps [33]. In addition to these lines, the He-like

Fig. 6. Experimental spectrum from the Zebra W/Mo X-pinch (top) and experimental M-shell spectrum of W ions from the LLNL EBIT-I electron ion beam trap recorded by the X-ray spectrometer microcalorimeter at $E_b = 3.9$ keV (bottom).

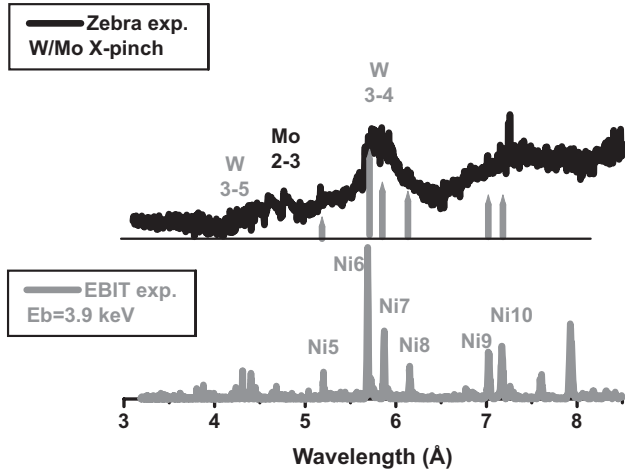


Fig. 7. Experimental combined Al/W (light grey) and W/Mo (black) X-pinch spectra fit with a synthetic spectrum from our model at $T_e = 1$ keV, $N_e = 10^{21}$ cm $^{-3}$, and $f = 0.03$ (grey).

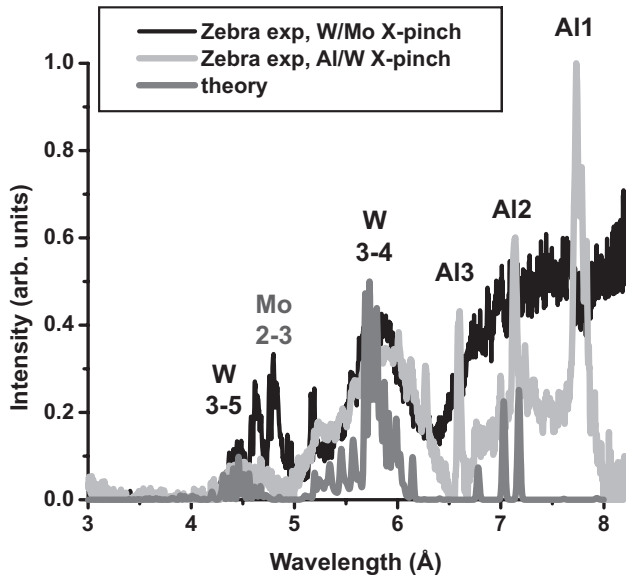


Table 2. K-shell Ti lines important in the diagnostics of low-density plasmas.

Iso-electronic sequence	Line	Transition		Wavelength λ (Å)
		Upper level	Lower level	
He-like	w	$1s2p^1P_1$	$1s^2^1S_0$	2.6105
He-like	x	$1s2p^3P_2$	$1s^2^1S_0$	2.6192
He-like	y	$1s2p^3P_1$	$1s^2^1S_0$	2.6229
Li-like	q	$1s2s2p^2P_{3/2}$	$1s^2s^2S_{1/2}$	2.6277
Li-like	r	$1s2s2p^2P_{1/2}$	$1s^2s^2S_{1/2}$	2.6300
He-like	z	$1s2s^3S_1$	$1s^2^1S_0$	2.6370

Table 3. Ratios of the K-shell Ti line intensities from LLNL EBIT experiments produced by a monoenergetic electron beam centered at 4.8 keV and a quasi-Maxwellian electron beam at $T_e=2.3$ keV.

	$E_b = 4800$ eV			$T_{max} = 2.3$ keV		
	Monoenergetic beam [34]			Quasi-Maxwellian beam [35]		
	Si(220)	Si(111)		Si(220)	Ge(111)	
	I_1	I_2	I_1/I_2	I_3	I_4	I_3/I_4
y/w	0.147	0.235	0.63	0.113	0.153	0.74
x/w	0.102	0.191	0.53	0.068	0.145	0.47
z/w	0.258	0.343	0.75	0.212	0.335	0.63
q/w	0.313	0.316	0.99	0.184	0.255	0.72

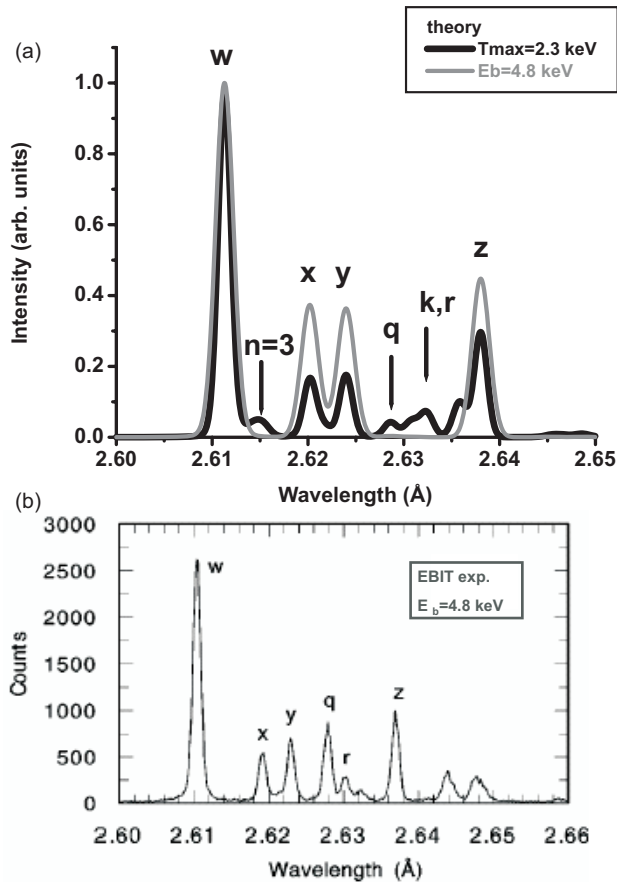
resonance line He β , the H-like resonance line Ly α , the satellite line of Be-like ions (Be) and the “cold” K α lines of Ti are used in the diagnostics of X-pinch plasmas. The data from two polarization-sensitive experiments at the LLNL EBIT will be considered. The first experiment involved the measurement of X-ray line polarization of K-shell Ti lines excited by a monoenergetic beam [34]. The polarization-sensitive X-ray spectrum of He-like Ti was produced at the energy just above the electron-impact excitation threshold, 4800 eV (and thus below the KMM dielectronic resonances). The measured intensities were simultaneously recorded by spectrometers with a Si (220) crystal, which records an almost pure parallel polarization state, and with a Si (111) crystal, which records a mixture of both polarization states [34]. In the second experiment the same technique was used, but the K-shell Ti spectra were generated by a quasi-Maxwellian electron beam [35, 36]. The details of the technique for producing a quasi-Maxwellian electron beam and its implementation at the LLNL EBIT facility can be found in refs. 37 and 38. In the second experiment [35, 36] the measured intensities were simultaneously recorded by spectrometers with a Si (220) crystal (observing an almost pure parallel polarization state) and with a Ge (111) crystal (observing a mixture of both polarization states). The ratios of the relative intensities of K-shell Ti lines from these two LLNL EBIT experiments are listed in Table 3. In the next section, we focus on the data from the two spectrometers employing Si (111) and Ge (111) crystals, which are the least sensitive to polarization, i.e., on the ratios I_2 and I_4 , respectively (see Table 3).

3.1. Modeling of X-ray K-shell Ti spectra

The non-LTE CR Ti model was applied to analyze K-shell Ti data (for the details of the model, see refs. 29 and 30). Briefly, this model is also based on atomic data calculated using the FAC code [19]. It includes the ground states of all ions; singly excited levels up to $n = 5$ for H- and He-like ions, $n = 4$ for Li-like ions, and $n = 3$ for Be-through Ne-like ions; and doubly-excited levels up to $n = 3$ for He-, Li-, and Ne-like ions, and up to $n = 2$ for Be through F-like ions. All levels are coupled by radiative decay and collisional excitation and de-excitation within each ion and by collisional ionization, Auger decay, and their reverse processes as well as by radiative recombination between neighboring ions [30].

In Fig. 8a theoretical synthetic spectra of K-shell Ti are shown calculated at low density for two different electron distribution functions (EDF): a Gaussian centered at 4.8 keV (gray line) and a Maxwellian at $T_M = 2.3$ keV (black line). The

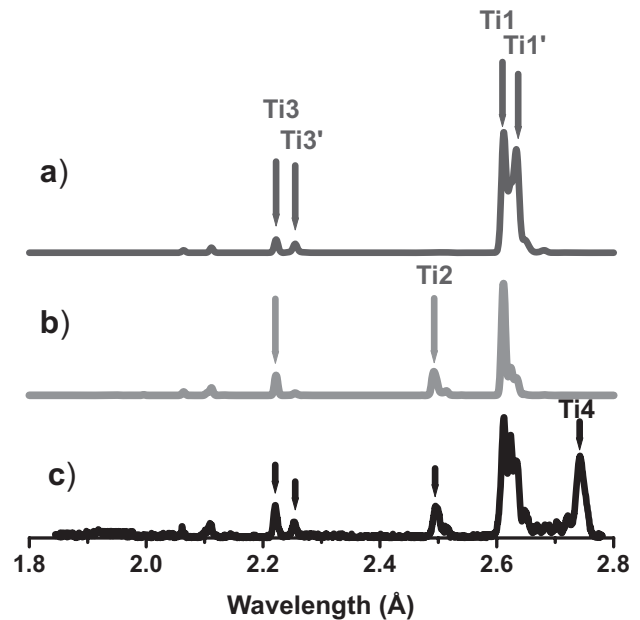
Fig. 8. (a). Theoretical synthetic spectra of K-shell Ti calculated at low density for two different electron distribution functions: a Gaussian of FWHM = 50 eV centered at 4.8 keV (grey line) and a Maxwellian at $T_M = 2.3$ keV (black line). (b). EBIT experimental spectrum produced by the monoenergetic electron beam at $E_b = 4800$ eV and recorded by a Si (111) crystal less sensitive to polarization (Fig. 1b from [34]).



theoretical spectrum calculated for a Gaussian EDF is compared with the EBIT experimental spectrum produced by the monoenergetic electron beam at $E_b = 4800$ eV and recorded by a Si (111) crystal from ref. 34 (see Fig. 8b). This crystal is less sensitive to polarization. Theory describes the EBIT experimental spectrum as well as ratios and differences in spectra between monoenergetic (Gaussian) and quasi-Maxwellian beams for lines x, y, and z well. In Fig. 8a, it is clear that the ratios x/w and y/w are more than 50% larger for the Gaussian EDF (I_2) than for the Maxwellian EDF (I_4) while the ratio z/w is almost unchanged. However, the modeling does not show any line q (Li-like inner-shell satellite at 2.6277 Å) for the Gaussian EDF which appeared to be $\sim 30\%$ of the w line in the experimental spectrum in Fig. 8b (see also Table 3). This problem is likely related to the fact that the charge balance in EBIT was shifted toward lower charge states in this measurements, and is not a polarization effect.

Now we will consider the K-shell Ti spectra produced by the 1 MA pulsed-power Zebra generator at UNR. A typical Ti X-pinch spectrum as well as our modeling results using the non-LTE CR Ti model mentioned above is shown in Fig. 9. The modeling of the Ti X-pinch spectrum indicates that the emission

Fig. 9. Theoretical synthetic spectra of K-shell Ti calculated at (a) $T_e = 1$ keV and $N_e = 10^{21}$ cm $^{-3}$ and (b) $T_e = 2.2$ keV and $N_e = 10^{22}$ cm $^{-3}$ are used for the interpretation of the typical Ti X-pinch spectrum (c) produced on Zebra at UNR.



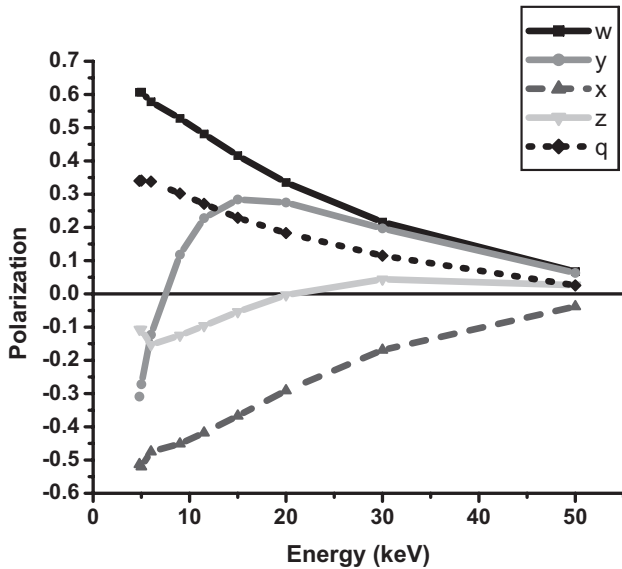
comes from at least two different regions: a hot dense region and a cooler and probably less dense region. In particular, the synthetic spectrum at the top (Fig. 9a) is calculated at $T_e = 1$ keV and $N_e = 10^{21}$ cm $^{-3}$ and represents the region of Ti plasma with intense He-like lines Ti1 (w, He α), Ti1' (y), Ti3 (He β), and the Li-like satellites Ti3'. The synthetic spectrum in the middle (Fig. 9b) is calculated at $T_e = 2.2$ keV and $N_e = 10^{22}$ cm $^{-3}$ and represents the hot and dense region with intense H-like line Ti2 (Ly α) as well as intense He-like lines Ti1 (w, He α) and Ti3 (He β). In addition to these two plasma regions, there may be the third region, which is even cooler than the first one. It emits radiation from Li-like, Be-like, and other lower-ionization ions. These satellites are located on the right from the line y at $\lambda > 2.625$ Å. The "cold" Ti K α line (Ti4) indicates the presence of very low-temperature plasma (~ 20 eV) and is not modeled here. The detailed temperature determination using the "cold" Ti K α line from laser-plasma interaction experiments is presented in ref. 39.

3.2. Polarization of X-ray line radiation: calculations and applications to experiment

Ti X-pinch experiments on the 1 MA Zebra at UNR provided experimental evidence of the existence of strong electron beams. This motivated the development of a new diagnostics, X-ray spectropolarimetry, for investigating the anisotropy of the plasma EDF. X-ray spectropolarimetry is based on the knowledge of the polarization properties of radiation. An excellent test bed for the study of X-ray line polarization and the benchmarking of the polarization-sensitive calculations (as was mentioned in the Introduction) is EBIT.

We begin with a calculation of the polarization of lines that will be applied to experiments at the LLNL EBIT and then to X-pinch experiments on Zebra at UNR. Values of the polarization of the most diagnostically important lines were calculated

Fig. 10. Polarization of the most intense K-shell Ti lines as a function of the electron beam energy. Identification of these lines is given in Table 2.



using the FAC code [19] and are presented in Fig. 10 and in Table 4. The lines listed in Table 2 are produced by the electron impact excitation, and thus their polarization is shown as a function of electron beam energy. The polarization of the most intense line w has its maximum ($\sim 60\%$) near the excitation threshold (~ 4.7 keV) and then gradually decreases towards zero and is less than 10% at ten times threshold. By contrast, the polarization of line y changes non-monotonically with the energy of the electron beam. It is negative near the threshold ($\sim -30\%$), then changes sign and becomes $\sim +30\%$ already at three times threshold. Then it approaches the polarization of the w line. Hence, when the measured polarization of the w and y lines is the same then the energy of the electron beam is higher than 30 keV and when it is different then it indicates a low-energy electron beam with the energy close to the threshold or only somewhat higher. This result is important in diagnosing the energy of beams in plasmas.

Table 4 gives the theoretical values of the degree of polarization for the K-shell Ti lines excited by a monoenergetic electron beam with an energy of 4.8 and 11.5 keV calculated using the FAC code. In addition, for $E_b = 4.8$ keV, the experimental values of polarization as well as theoretical predictions from ref. 34 are listed. Experimental values in ref. 34 were obtained using the measured intensities (see Table 3) and a two-crystal technique [40]. The ratio of intensities I_1/I_2 from Table 3 close to 1 indicates almost equal values for the polarization of the two lines. For example, this ratio $I_1/I_2 = 0.99$ for q/w (see Table 3) and corresponding degrees of polarization for lines w and q are both ~ 0.4 (see Table 4). The ratio of intensities $I_1/I_2 = 0.75$ for z/w and the corresponding degree of polarization of the line z is -0.101 . The smallest ratio of $I_1/I_2 = 0.53$ for x/w results in the most negative value of polarization of this line (-0.48). Our values calculated for $E_b = 4.8$ keV agree well with the measured and theoretical values from ref. 34.

The theoretical values of the polarization calculated at $E_b = 4.8$ and 11.5 keV show limits within which the polarization

Table 4. Polarization degrees for the K-shell Ti lines excited by monoenergetic electron beams with the energy $E_b = 4.8$ and 11.5 keV calculated using the FAC code. The values of polarization degrees for $E_b = 4.8$ keV are compared with results of ref. 34.

	$E_b = 4.8$ keV		$E_b = 11.5$ keV	
	Theory	Theory	Expt.	Theory
	Present paper	Ref. 34	Ref. 34	Present paper
w	+0.607	+0.608	$+0.43^{+0.14}_{-0.12}$	+0.481
y	-0.309	-0.339	$-0.33^{+0.07}_{-0.07}$	+0.228
x	-0.513	-0.519	$-0.48^{+0.06}_{-0.06}$	-0.418
z	-0.106	-0.106	$-0.101^{+0.014}_{-0.013}$	-0.096
q	+0.340	+0.341	$+0.40^{+0.15}_{-0.10}$	+0.270

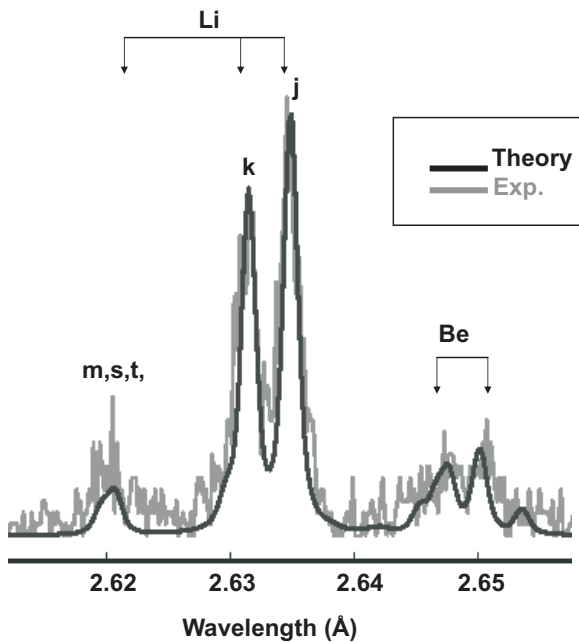
is changing in the experiment with a quasi-Maxwellian electron beam (the second experiment discussed in the beginning of this section). As was discussed before, polarization of the line y changes the most (from -0.308 to $+0.228$), which may result in almost zero polarization. The polarization of the other lines changes only slightly, in particular, decreases for positively polarized lines (w and q) and increases for the negatively polarized lines (z and x). To employ the two-crystal technique from refs. 34 and 40, we need to make an assumption about the value of the polarization of a certain line. If we assume the polarization of the line w is 0.5 then using eq. (2.5) from ref. 34 and the polarization-sensitive ratios I_3/I_4 for the lines y, z, and x, we estimate polarization of almost zero for the line y ($I_3/I_4 = 0.74$), ~ -0.2 for the line z ($I_3/I_4 = 0.63$), and ~ -0.48 for the line x ($I_3/I_4 = 0.47$). These values for the polarization fall within the corresponding limits from Table 4. They also correlate well with the above analysis of the intensity ratios I_1/I_2 from Table 3. On the contrast, the estimate for polarization of the line q gives a small negative value that does not agree with our prediction (see Table 4). This will be a subject of future work.

In a Maxwellian plasma dielectronic satellite transitions play an important role and several $n = 2$ satellites produced by the processes $1s^2 + e^- \rightarrow 1s2l2l'$ and $1s^22s + e^- \rightarrow 1s2s2l2l'$ are seen. These satellite lines are produced within the narrow band of energies and, therefore, sample EDF at very close energies (~ 3.3 keV) while the line w integrates the EDF from the excitation threshold (~ 4.7 keV) and up to the highest energies. For example, the most intense dielectronic satellite lines j and k are produced at the energies of 3327.3 and 3325.9 eV, respectively [41]. Using the event-mode data acquisition technique [37, 42] allows us to select only the photons with energies close to ~ 3.3 keV produced in the same experiment that produced the spectrum in Fig. 8a. Because the energy is well below 4.7 keV the lines w, y, and z are not seen in the spectrum. This is illustrated in Fig. 11 where we show the dielectronic satellite spectra of Li-like (lines j, k, s, m, and t) and Be-like Ti recorded by the Si (220) crystal in the experiment with a quasi-Maxwellian electron beam from ref. 36. As was mentioned before, this crystal was the most sensitive to polarization and was recording almost pure parallel polarization states. The theoretical polarization-sensitive spectra describe the experiment well. The details of calculations of atomic and polarization characteristics of these transitions in Ti ions are given in ref. 41.

Table 5. Measured values of the intensities of lines recorded by a horizontal (H) and a vertical (V) spectrometers in Ti X-pinch experiments.

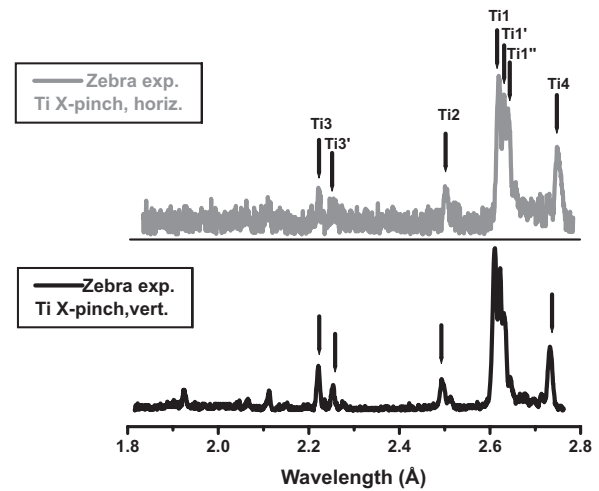
Iso-elect. seq.	Line	Shot 36			Shot 37			Shot 39		
		H	V	H/V	H	V	H/V	H	V	H/V
He-like	Ti1 (w)	2.19[7]	1.90[7]	1.15	2.79[7]	2.68[7]	1.04	2.97[7]	3.66[7]	0.81
He-like	Ti1'(y)	1.98[7]	1.58[7]	1.25	2.38[7]	2.08[7]	1.14	2.62[7]	3.21[7]	0.82
Li-like	Ti1''(q)	1.69[7]	1.30[7]	1.30	1.79[7]	1.54[7]	1.16	2.36[7]	2.20[7]	1.07
Be-like	Ti1'''	6.48[6]	5.23[6]	1.24	6.47[6]	5.22[6]	1.24	9.81[6]	7.34[6]	1.34
Low ioniz.	Ti4 (K_{α})	2.30[7]	2.24[7]	1.03	1.90[7]	1.64[7]	1.16	1.64[7]	1.43[7]	1.15

Fig. 11. Comparison of experimental (grey line) and theoretical (black line) dielectronic recombination spectra of K-shell Ti. The experimental spectrum was produced on LLNL EBIT recorded with a von Hámos type crystal spectrometer employing a Si (220) crystal which allowed an almost pure parallel polarization state.



The K-shell line radiation from Ti X-pinch was recorded by a polarimeter, which includes so-called horizontal (H) and vertical (V) spectrometers. The experimental details including the diagnostic setup were described in refs. 15 and 43. Briefly, the “H” spectrometer has a dispersion plane perpendicular to the discharge axis and records mostly the parallel polarization state. The “V” spectrometer has a dispersion plane parallel to the discharge axis and records mostly the perpendicular polarization state. Both “H” and “V” spectrometers were two identical convex crystal spectrometers utilizing LiF crystals with a lattice spacing ($2d = 4.027 \text{ \AA}$) corresponding to nominal Bragg angles from 40.6° (for Ti1 line) up to 42.9° (for Ti4 line). Typical spectra recorded by the “H” and “V” spectrometers are presented in Fig. 12 (shot 39). The experimental intensity ratios of the K-shell Ti lines with the wavelengths providing the Bragg angle closest to 45° (Ti1, Ti1', Ti1'', Ti1''', and Ti4) are listed in Table 5 for three selected shots where Ti X-pinch was made from $30 \mu\text{m}$ Ti wires. The experimental intensity ratios in Table 5 are associated with different polarization states I_{\parallel}/I_{\perp} for each of the spectral lines from the horizontal and vertical spectra (H/V). A ratio I_{\parallel}/I_{\perp} greater (less) than unity for a

Fig. 12. Polarization-sensitive K-shell spectra from a Ti X-pinch produced on Zebra at the University of Nevada, Reno. The spectra were simultaneously recorded by the horizontal (top) and vertical (bottom) spectrometers (Zebra shot 39).



given line indicates positive (negative) polarization of the line. We believe that line polarization occurred in shot 39, where the largest deviations from unity have been observed. For this particular shot, for He-like lines Ti1 and Ti1' the ratio H/V is less than or equal to one (i.e., negative polarization). It indicates the energy of electron beams was higher than 30 keV (see Fig. 10). More experimental data are needed to refine this technique to estimate line polarization and energy of electron beams with sufficient accuracy.

In addition to the resonance lines and satellite lines the relative intensities of the “cold” Ti K_{α} line (from wire material) and the “cold” Fe K_{α} line (from the stainless steel anode) were measured [15]. It was shown that the relative intensities of both “cold” lines have their minimum values for shot 39 when the largest polarization was observed. This means that observation of strong characteristic lines does not necessarily indicate the presence of electron beams responsible for line polarization. It would be interesting to study the polarization of the “cold” Ti K_{α} line and its application for Z-pinch plasma diagnostics.

4. Conclusion

The development of X-ray diagnostics of Z-pinch plasmas during the last six years was reviewed. This development was focused on the M-shell emission of W and the K-shell emission of Ti. High-temperature and high-density plasmas were produced from the variety of X-pinch on the 1 MA Zebra de-

vice at UNR. In particular, M-shell W radiation was generated by the implosions of X-pinchs with tungsten wires combined with the wires from other lower Z wire material such as Al and Mo. The M-shell emission of W ions is a very challenging topic for plasma diagnostics because of contributions from numerous ionization stages in a narrow spectral region that is impossible to resolve. LLNL EBIT data produced at various beam energies and recorded by a high-resolution crystal spectrometer and a broadband microcalorimeter allowed us to break down this very complicated M-shell spectrum into spectra with a limited number of ionization stages. LLNL EBIT data helped not only to identify the spectra from X-pinchs but also to benchmark the theoretical modeling.

The results of polarization-sensitive experiments with Ti X-pinchs on the Zebra at UNR were also reviewed. It was shown that the difference in polarization-dependent spectra provided information about the existence of electron beams in Z-pinch plasmas. Refinement of the technique should also provide a value of the average energy of the beams. Polarization-dependent spectra of the Ti K-shell emission that were generated by a quasi-Maxwellian beam at the LLNL EBIT facility were studied, and the usefulness of these data for X-ray spectropolarimetry was emphasized. Also the importance of the ability of EBIT to simulate a quasi-Maxwellian beam for bench-marking theoretical calculations was demonstrated.

Acknowledgement

This work was supported by the National Nuclear Security Administration under Department of Energy Cooperative Agreement DE-FC52-06NA27588 and in part by DE-FC52-06NA27586. Work at the Lawrence Livermore National Laboratory was performed under of auspices of the Department of Energy under contract No. W-7405-Eng-48.

References

- [1] P.G. Burkhalter, C.M. Dozier, and D.J. Nagel. *Phys. Rev. A*, **15**, 700 (1977).
- A. Zigler, H. Zmora, N. Spector, M. Klapisch, J.L. Schwob, and A. Bar-Shalom. *J. Opt. Soc. Am.* **70**, 129 (1980).
- N. Tragin, J.-P. Geindre, P. Monier, J.C. Gauthier, C. Chenais-Popovics, J.-F. Wyart, C. Bauche-Arnoult. *Phys. Scr.* **37**, 72 (1988).
- R.B. Spielman, C. Deeney, G.A. Chandler, M.R. Douglas, D.L. Fehl, M.K. Matzen, D.H. McDaniel, T.J. Nash, J.L. Porter, T.W.L. Sanford, J.F. Seamen, W.A. Stygar, K.W. Struve, S.P. Breeze, J.S. McGurn, J.A. Torres, D.M. Zagar, T.L. Gilliland, D.O. Jobe, J.L. McKenney, R.C. Mock, M. Vargas, and T. Wagoner. *Phys. Plasmas*, **5**, 2105 (1998).
- C. Deeney, M.R. Douglas, R.B. Spielman, T.J. Nash, D.L. Peterson, P.L. 'Eplattienier, G.A. Chandler, J.F. Seamen, and K.W. Struve. *Phys. Rev. Lett.* **81**, 4883 (1998).
- M.E. Cuneo, R.A. Vesey, J.L. Porter, Jr., G.R. Bennett, D.L. Hanson, L.E. Ruggles, W.W. Simpson, G.C. Idzorek, W.A. Stygar, J.H. Hammer, J.J. Seamen, J.A. Torres, J.S. McGurn, and R.M. Green. *Phys. Rev. Lett.* **88**, 215004 (2002).
- M.E. Cuneo, E.M. Waisman, S.V. Lebedev, J.P. Chittenden, W.A. Stygar, G.A. Chandler, R.A. Vesey, E.P. Yu, T.J. Nash, D.E. Bliss, G.S. Sarkisov, T.C. Wagoner, G.R. Bennett, D.B. Sinars, J.L. Porter, W.W. Simpson, L.E. Ruggles, D.F. Wenger, C.J. Garasi, B.V. Oliver, R.A. Aragon, W.E. Fowler, M.C. Hettrick, G.C. Idzorek, D. Johnson, K. Keller, S.E. Lazier, J.S. McGurn, T.A. Mehlhorn, T. Moore, D.S. Nielsen, J. Pyle, S. Speas, K.W. Struve, and J.A. Torres. *Phys. Rev. E*, **71**, 046406 (2005).
- V.L. Kantsyrev, A.S. Safronova, V.V. Ivanov, D. Fedin, R. Mancini, A. Astanovitsky, B. LeGalloudec, S. Batie, D. Brown, V. Nalajala, I. Shrestha, S. Pokala, N. Ouart, F. Yilmaz, A. Clinton, M. Johnson, T. Cowan, B. Jones, C.A. Coverdale, C. Deeney, P.D. LePell, D. Jobe, and D. Nielson. *J. Quant. Spectrosc. Radiat. Transfer*, **99**, 349 (2006).
- A.S. Safronova, V.L. Kantsyrev, N.D. Ouart, F. Yilmaz, D. Fedin, A. Astanovitsky, B. LeGalloudec, S. Batie, D. Brown, V. Nalajala, S. Pokala, I. Shrestha, T. E. Cowan, C.A. Coverdale, C. Deeney, S.B. Hansen, P.D. LePell, D. Jobe, and D. Nielson. *J. Quant. Spectrosc. Radiat. Transfer*, **99**, 560 (2006).
- V.L. Kantsyrev, A.S. Safronova, D.A. Fedin, V. V. Ivanov, A.A. Esaulov, V. Nalajala, I. Shrestha, S. Pokala, K. Williamson, N.D. Ouart, M.F. Yilmaz, P. Laca, T.E. Cowan, L.I. Rudakov, B. Jones, C.A. Coverdale, C. Deeney, P.D. LePell, A.L. Velikovich, and A.S. Chuvatin. *IEEE Trans. Plasma Sci.* **34**, 194 (2006).
- A. Safronova, V. Kantsyrev, D. Fedin, F. Yilmaz, T. Hoppe, V. Nalajala, J. Douglass, R. McBride, M. Mitchell, L. Maxson, and D. Hammer. *AIP Conf. Proc.* **808**, 145 (2006).
- A. Safronova, V. Kantsyrev, D. Fedin, F. Yilmaz, T. Hoppe, V. Nalajala, J. Douglass, R. McBride, M. Mitchell, L. Maxson, and D. Hammer. *IEEE Trans. Plasma Sci.* **34**, 2256 (2006).
- T.A. Shelkovenko, D.B. Sinars, S.A. Pikuz, and D.A. Hammer. *Phys. Plasmas*, **8**, 1305 (2001).
- V.L. Kantsyrev, D.A. Fedin, A.S. Shlyaptseva, S. Hansen, D. Chamberlain, and N. Ouart. *Phys. Plasmas*, **10**, 2519 (2003).
- A.S. Shlyaptseva, V.L. Kantsyrev, N. Ouart, D. Fedin, S. Hamasha, and S. Hansen. *Proc. SPIE*, **5196**, 16 (2004).
- A.S. Shlyaptseva, R.C. Mancini, P. Neill, and P. Beiersdorfer. *Rev. Sci. Instrum.* **68**, 1095 (1997).
- A.S. Shlyaptseva, R.C. Mancini, P. Neill, P. Beiersdorfer, J.R. Crespo López-Urrutia, and K. Widmann. *Phys. Rev. A*, **57**, 888 (1998).
- A.S. Shlyaptseva, R.C. Mancini, P. Neill, and P. Beiersdorfer. *J. Phys. B*, **32**, 1041 (1999).
- M.F. Gu. *AIP Conf. Proc.* **730**, 127 (2004).
- H.V. Regemorter. *Astrophys. J.* **136**, 906 (1962).
- V.A. Bernshtam, Yu.V. Ralchenko, and Y. Maron. *J. Phys. B*, **33**, 5025 (2000).
- S.M. Hamasha, A.S. Shlyaptseva, and U.I. Safronova. *Can. J. Phys.* **82**, 331 (2004).
- U.I. Safronova, A.S. Safronova, S.M. Hamasha, and P. Beiersdorfer. *At. Data Nucl. Data Tables*, **96**, 47 (2006).
- U.I. Safronova, A.S. Safronova, and P. Beiersdorfer. *J. Phys. B*, **39**, 4491 (2006).
- P. Neill, C. Harris, A.S. Safronova, S.M. Hamasha, S.B. Hansen, P. Beiersdorfer, and U.I. Safronova. *Can. J. Phys.* **82**, 931 (2004).
- A.S. Shlyaptseva, D.A. Fedin, S.M. Hamasha, C. Harris, V.L. Kantsyrev, P. Neill, N. Ouart, U.I. Safronova, P. Beiersdorfer, K. Boyce, G.V. Brown, R. Kelley, C.A. Kilbourne, and F.S. Porter. *Rev. Sci. Instrum.* **75**, 3750 (2004).
- F.S. Porter, G.V. Brown, K.R. Boyce, R.L. Kelley, C.A. Kilbourne, P. Beiersdorfer, H. Chen, S. Terracol, S.M. Kahn, and A.E. Szymkowiak. *Rev. Sci. Instrum.* **75**, 3772 (2004).

28. F.S. Porter, B.R. Beck, P. Beiersdorfer, K.R. Boyce, G.V. Brown, H. Chen, J. Gygax, S.M. Kahn, R.L. Kelley, C.A. Kilbourne, E. Magee, and D.B. Thorn. *Can. J. Phys.* **86** (2008). This issue.
29. S.B. Hansen. Ph.D. Dissertation, University of Nevada, Reno. 2003.
30. S.B. Hansen and A.S. Shlyaptseva. *Phys. Rev. E*, **70**, 036402 (2004).
31. M. Bitter, K.W. Hill, M. Zarnstorff, S. von Goeler, R. Hulse, L.C. Johnson, N.R. Sauthoff, S. Sesnic, K.M. Young, M. Tavernier, F. Bely-Dubau, P. Faucher, M. Cornille, and J. Dubau. *Phys. Rev. A*, **32**, 3011 (1985).
32. P. Lee, A.J. Lieber, R.P. Chase, and A.K. Pradhan. *Phys. Rev. Lett.* **55**, 386 (1985).
33. P. Beiersdorfer, V. Decaux, S.R. Elliott, K. Widmann, and K. Wong. *Rev. Sci. Instrum.* **66**, 303 (1995).
34. P. Beiersdorfer, G. Brown, S. Utter, P. Neill, A.J. Smith, and R.S. Thoe. *Phys. Rev. A*, **60**, 4156 (1999).
35. A.S. Shlyaptseva, D.A. Fedin, S.M. Hamasha, S.B. Hansen, C. Harris, V.L. Kantsyrev, P. Neill, N. Ouart, P. Beiersdorfer, and U.I. Safronova. *Rev. Sci. Instrum.* **74**, 1947 (2003).
36. A.S. Shlyaptseva, V.L. Kantsyrev, B.S. Bauer, P. Neill, C. Harris, D.A. Fedin, S. Hansen, N. Ouart, P. Beiersdorfer, A.G. Petrashen, and U.I. Safronova. Proceedings of the 3rd PPS Workshop. *Edited by* P. Beiersdorfer and T. Fujimoto. University of California LLNL Rep. No. UCRL-ID-146907, 339 (2001).
37. D.W. Savin, P. Beiersdorfer, S.M. Kahn, B.R. Beck, G.V. Brown, M.F. Gu, D.A. Liedahl, and J.H. Scofield. *Rev. Sci. Instrum.* **71**, 3362 (2000).
38. D.W. Savin, N.R. Badnell, P. Beiersdorfer, B.R. Beck, G.V. Brown, P. Bryans, T.W. Gorczyca, M.F. Gu, and S.M. Kahn. *Can. J. Phys.* **86** (2008). This issue.
39. S.B. Hansen, A.Ya. Faenov, T.A. Pikuz, K.B. Fournier, R. Shepherd, H. Chen, K. Widmann, S.C. Wilks, Y. Ping, H.K. Chung, A. Niles, J.R. Hunter, G. Dyer, and T. Ditmire. *Phys. Rev. E*, **72**, 036408 (2005).
40. P. Beiersdorfer, D.A. Vogel, K.J. Reed, V. Decaux, J.H. Scofield, K. Widmann, G. Hölzer, E. Förster, O. Wehrhan, D.W. Savin, and L. Schweikhard. *Phys. Rev. A*, **53**, 3974 (1996).
41. A.S. Shlyaptseva, S. Hansen, V.L. Kantsyrev, S. A. Kazantsev, A.G. Petrashen, and U.I. Safronova. Proceedings of the 3rd PPS Workshop. *Edited by* P. Beiersdorfer and T. Fujimoto. University of California LLNL Rep. No. UCRL-ID-146907, 93 (2001).
42. D.A. Knapp, R.E. Marrs, M.B. Schneider, M.H. Chen, M.A. Levine, and P. Lee. *Phys. Rev. A*, **47**, 2039 (1993).
43. A.S. Shlyaptseva, V.L. Kantsyrev, N.D. Ouart, D.A. Fedin, P. Neill, C. Harris, S.M. Hamasha, S.B. Hansen, U.I. Safronova, P. Beiersdorfer, A.G. Petrashen. Proceedings of the 4th PPS Workshop. *Edited by* T. Fujimoto and P. Beiersdorfer. NIFS-PROC **57**, 47 (2004).